Aldehyde Oxidase Contributes to all-*trans*-Retinoic Acid Biosynthesis in Human Liver

Guo Zhong, Chris J. Seaman, Erickson M. Paragas, Huaqing Xi, Karla-Luise Herpoldt, Neil King, Jeffrey P. Jones, Nina Isoherranen*

Department of Pharmaceutics, School of Pharmacy, University of Washington, Seattle, WA (G.Z., CJ.S., H.X., N.I.);

Department of Chemistry, Washington State University, Pullman, WA (EM.P, J.J.);

Department of Biochemistry and Institute for Protein Design, University of Washington, Seattle, WA (K.H., N.K.).

* Corresponding author

Corresponding Author: Nina Isoherranen, Department of Pharmaceutics, School of Pharmacy, University of Washington, Health Science Building, Room H-272M, Box 357610, Seattle, Washington 98195-7610 USA, Phone: 206-543-2517; Fax: 206-543-3204; Email: ni2@uw.edu

Running title: Retinoic acid synthesis by aldehyde oxidase

Text Pages: 19

Tables: 2

Figures: 5

References: 31

Words in Abstract: 252

Words in Introduction: 559

Words in Discussion: 1302

Abbreviations:

ACN, acetonitrile; afe, average fold error; ALDH1A, aldehyde dehydrogenase 1A; AOX, aldehyde oxidase; *at*RA, all-*trans*-retinoic acid; CL_{int}, intrinsic clearance; CRBP, cellular retinol binding protein; FA, formic acid; f_m, fraction metabolized; HLS9, human liver S9 fraction; IS, internal standard; ISEF, intersystem extrapolation factor; K_m, Michaelis-Menten constant; KPi, potassium phosphate; MRM, multiple-reaction monitoring; RDH, retinol dehydrogenase; SIL-peptide, stable isotope-labeled peptide; v, velocity.

Abstract

All-*trans*-retinoic acid (*at*RA) is a critical endogenous signaling molecule. *at*RA is predominantly synthesized from retinaldehyde by aldehyde dehydrogenase 1A1 (ALDH1A1) but aldehyde oxidase (AOX) may also contribute to *at*RA biosynthesis. The goal of this study was to test the hypothesis that AOX contributes significantly to *at*RA formation in human liver. Human recombinant AOX formed *at*RA from retinaldehyde (K_m~1.5 ± 0.4 μM; k_{cat} ~3.6 ± 2.0 min^{-1}). In human liver S9 fractions (HLS9) *at*RA formation was observed in the absence of NAD^+, suggesting AOX contribution to *at*RA formation. In the presence of NAD^+, Eadie-Hofstee plots of *at*RA formation in HLS9 indicated that two enzymes contributed to *at*RA formation. The two enzymes were identified as AOX and ALDH1A1 based on inhibition of *at*RA formation by AOX inhibitor hydralazine (20-50% inhibition) and ALDH1A1 inhibitor WIN18,446 (50-80% inhibition). The expression of AOX in HLS9 was 9.4-24 pmol mg^{-1}S9 protein while ALDH1A1 expression was 156-285 pmol mg^{-1}S9 protein measured by LC-MS/MS quantification of signature peptides. The formation velocity of *at*RA in the presence of NAD^+ correlated significantly with the expression of ALDH1A1 and AOX protein. Taken together the data show that both AOX and ALDH1A1 contribute to *at*RA biosynthesis in the human liver with ALDH1A1 being the high affinity low capacity enzyme and AOX the low affinity high capacity enzyme. The results suggest that in the case of ALDH1A dysfunction or excess vitamin A, AOX may play an important role in regulating hepatic vitamin A homeostasis and that inhibition of AOX may alter *at*RA biosynthesis and signaling.

Significance statement: This study provides direct evidence to show that human AOX converts retinaldehyde to *at*RA and contributes to hepatic *at*RA biosynthesis. The finding that AOX may be responsible for 20-50% of overall hepatic *at*RA formation suggests that alterations in AOX activity via drug-drug interactions, genetic polymorphisms or disease states may impact hepatic *at*RA concentrations, signaling and alter vitamin A homeostasis.

Keywords: aldehyde oxidase, aldehyde dehydrogenase 1A1, all-*trans* retinoic acid, human liver, fraction metabolized

Introduction

Vitamin A (retinol) is an essential endogenous compound in all chordates. Retinol is first oxidized by retinol dehydrogenases (RDHs) to yield all-*trans*-retinaldehyde, which is further metabolized to all-*trans*-retinoic acid (*at*RA) (Napoli, 2012; Kedishvili, 2013). The active retinoid *at*RA binds to retinoic acid receptors and regulates various physiological processes, such as cell differentiation, T cell activation, spermatogenesis and lipid and glucose metabolism (Kedishvili, 2013). Liver, the major vitamin A storage organ, is an important site of retinoid metabolism. Aldehyde dehydrogenase 1A1 (ALDH1A1), one of the three members in the ALDH1A family, is believed to be the major enzyme responsible for *at*RA biosynthesis in the liver, and the enzyme activity is NAD^+ dependent (Arnold, Kent, Hogarth, Griswold, *et al.*, 2015; Arnold *et al.*, 2016). However, neither chemical inhibition of Aldh1a1 by WIN18,446 (Arnold, Kent, Hogarth, Griswold, *et al.*, 2015) nor global knockout of $Aldh1a1^{-/-}$ (Fan *et al.*, 2003) in mice completely abolish liver *at*RA biosynthesis. WIN18,446 inhibited 44% of *at*RA formation in mouse liver (Arnold, Kent, Hogarth, Griswold, *et al.*, 2015) and $Aldh1a1^{-/-}$ mice are healthy and fertile at adulthood with similar hepatic *at*RA concentrations as wild type mice (Fan *et al.*, 2003). Taken together, these findings suggest that other enzyme(s) contribute to hepatic *at*RA formation and maintenance of vitamin A homeostasis.

It has been proposed that aldehyde oxidase (AOX) contributes to *at*RA biosynthesis in select organs including the liver. AOX is a cytosolic enzyme expressed in most animals and encoded by a single gene in humans. AOX generally metabolizes aldehydes and N-containing heterocyclic compounds (Pryde *et al.*, 2010; Rashidi and Soltani, 2017), but unlike ALDH1As, catalysis by AOX does not require the cofactor NAD^+. AOX enzymes in rabbit and mouse liver have been reported to catalyze retinaldehyde oxidation to yield *at*RA (Tomita *et al.*, 1993; Huang *et al.*, 1999). The data that retinaldehyde concentrations increased in harderian gland of $Aox4^{-/-}$ mice and *at*RA concentrations decreased in the harderian gland and skin of $Aox4^{-/-}$ mice in comparison to wild type mice (Terao *et al.*, 2009) suggest that AOX may play an important role in regulating *at*RA biosynthesis. The AOX family of enzymes has also been reported to be involved in testicular *at*RA biosynthesis in mice (Beedle *et al.*, 2019) and hydralazine, an AOX inhibitor, decreased *at*RA formation in mouse liver S10 fractions by 45% (Arnold, Kent, Hogarth, Griswold, *et al.*, 2015). Furthermore, both NAD^+-dependent and independent retinaldehyde metabolism was observed in soluble extracts of human liver and kidney

(Ambroziak *et al.*, 1999), strongly suggesting that AOX is involved in *at*RA biosynthesis. Yet, AOX is not typically included when *at*RA formation is considered. This is largely due to the lack of *Aox* knockout mouse models. The only available *Aox4*$^{-/-}$ mouse model did not show any major morphological abnormalities or lethal phenotype that would be expected if *at*RA biosynthesis was significantly impaired (Terao *et al.*, 2009, 2020). In addition, at present no quantitative characterization of AOX contribution to *at*RA biosynthesis in specific tissues has been published. In this study we hypothesized that aside from ALDH1A1, AOX makes a significant contribution to *at*RA formation in human liver. We aimed to quantitatively characterize *at*RA formation mediated by AOX in human liver and delineate the relative contribution of ALDH1A1 and AOX in hepatic *at*RA formation. This characterization is important for addressing altered *at*RA synthesis in human liver in various disease states and due to drug-drug interactions.

Materials and Methods

Chemicals, reagents, tissues and recombinant enzymes

Retinaldehyde, *at*RA, *at*RA-d_5, NAD^+, NADPH, raloxifene and hydralazine were purchased from Millipore Sigma (Burlington, MA). WIN 18,446 was from Acros Organics (Geel, Belgium). All LC/MS grade solvents were purchased from Thermo Fisher Scientific (Waltham, MA). Pooled human liver S9 fractions (lot number 3212595, 27 donors with 12 male and 15 female) were purchased from Corning (Corning, NY). Human liver samples from three individual donors, HL136 (39 years old, Caucasian male), HL146 (10 years old Caucasian male) and HL149 (63 years old Caucasian female), were obtained from the tissue bank of University of Washington School of Pharmacy.

Expression and purification of recombinant human ALDH1A1, AOX and cellular retinol binding protein 1 (CRBP1) and preparation of human liver S9 fractions (HLS9)

Recombinant human AOX was expressed, purified and quantified as published previously (Barr *et al.*, 2013; Paragas *et al.*, 2017). Human recombinant ALDH1A1 was expressed in *E.coli* as previously described (Arnold, Kent, Hogarth, and Isoherranen, 2015) with several modifications. Briefly, frozen cell pellets were thawed on ice, resuspended with 25 ml lysis buffer (1 mg/ml of lysozyme, 500 mM NaCl, 20 mM Tris, 5 mM imidazole, pH7.4), and lysed at room temperature for 15 minutes with gentle shaking. Resuspended mixture was

centrifuged at 18,000 g for 20 minutes. The supernatant was loaded into a HisTrap HP column (GE Healthcare BioSciences, Marlborough, MA) using Biologic DuoFlow chromatography system (Bio-Rad Laboratories, Hercules, CA). The column was washed with 5x column volumes of wash buffer (20 mM Tris-HCl, 500 mM NaCl, 20 mM imidazole, pH 7.4) and ALDH1A1 was eluted with 5 column volumes of elution buffer (20 mM Tris-HCl, 500 mM NaCl, 300 mM imidazole, pH7.4). Fractions containing ALDH1A1 were concentrated and exchanged into HEDK buffer (10 mM Hepes-NaOH, 0.1 mM EDTA, 0.5 mM DTT, 100mM KCl, pH 8.0) using a HiLoad® 16/60 Superdex200 column (GE Healthcare Bio-Sciences, Marlborough, MA) following manufacturer's instructions. After the protein concentration was determined by a bicinchoninic acid (BCA) protein assay (Thermo Fisher Scientific, Waltham, MA), purified ALDH1A1 was stored at -20°C in HEDK buffer with 2 mM tris(2-carboxyethyl)phosphine and 50% glycerol.

The gene encoding CRBP1 was ordered from Integrated DNA Technologies (Coralville, IA, USA) as a gBlock and cloned into pET28b (Novagen, Madison, WI, USA) using Gibson assembly between the NdeI and XhoI endonuclease restriction sites. Cloning at this site incorporates an N-terminus, thrombin cleavable, His-Tag. The DNA and amino acid sequences are listed in Table S1. The plasmid encoding CRBP-1 was then transformed into the T7 Express strain of *E. coli* (New England Biolabs, Ipswich, ME, USA) for protein expression. Cells were grown in LB medium supplemented with 50 mg/L of kanamycin at 37° C until an OD_{600} of 0.6 was reached. Protein expression was induced by addition isopropyl-thio-β-D-galactopyranoside to a final concentration of 1 mM. After induction, cells were allowed to grow for 16 hours at 18 °C before harvesting by centrifugation. Cells pellets were lysed by sonication (2.5 minutes in 2 s pulses) in 50 mM Tris pH 8, 150 mM NaCl, 20 mM imidazole, 0.05 mg/mL DNase, 0.05 mg/mL RNase, and 1 mM phenylmethylsulfonyl fluoride (PMSF). Lysate was centrifuged at 25,000 g for 25 min. Lysate supernatants were applied to HisTrap FF columns (GE Healthcare, Uppsala, Sweden) for purification by immobilized metal affinity chromatography (IMAC) on an AKTA Pure FPLC system (GE Healthcare, Uppsala, Sweden). The protein of interest was eluted over a linear gradient of 20 mM to 500 mM imidazole in a background of 50 mM Tris pH 8, 150 mM NaCl, after washing with ~10 column volumes wash buffer (elution buffer with 20 mM imidazole). Peak fractions were concentrated in 3K MWCO centrifugal filters, sterile filtered (0.22 μm) and dialyzed overnight to remove imidazole into a buffer containing 25 mM Tris pH

8, 150 mM NaCl. Following dialysis, thrombin was added at a dilution of 1:2000 (v/v) and incubated overnight at 4 °C. To remove cleaved His-Tag fragments and any un-cleaved protein, the solution was applied to an equilibrated HisTrap FF column and the flow-through collected. The collected protein was again concentrated using a 3K MWCO centrifugal filter and applied to a Superdex 200 Increase 10/300 GL SEC column (GE Healthcare, Uppsala, Sweden) using 25 mM Tris pH 8, 150 mM NaCl. Purified CRBP1 was stored at -20°C with 20% glycerol.

To prepare HLS9 fractions, liver samples (140-170 mg) from three donors were homogenized on ice with homogenizing buffer (50 mM potassium phosphate (KPi) containing 250 mM sucrose and 50 mM KCl, pH 7.4) in a 5 to 1 ratio of buffer to liver weight. After centrifugation at 9,000 g at 4℃ for 30 min, the supernatant (HLS9) was collected, aliquoted and stored at -80 ℃ until use. The protein concentration in each human liver S9 sample was measured using a BCA protein assay (Thermo Fisher Scientific, Waltham, MA).

General protocol of enzyme incubations and *at*RA quantification using LC-MS/MS

Incubations were performed according to the following protocol unless otherwise stated: HLS9 or purified recombinant enzymes were first pre-incubated at 37°C for 3 min in 100 mM KPi buffer (pH7.4) in a final volume of 100 µL. The reactions were initiated by adding retinaldehyde. The incubation times were as described for each experiment in the following sections. When possible 30 sec incubation time was used to avoid substrate depletion and time dependent loss of enzyme activity. In incubations which had low product formation rates due to chemical inhibition or low enzyme expression, longer incubation periods (up to 3 min) were employed to allow sufficient sensitivity and detection of *at*RA formation while maintaining incubation time within the linear range. All the incubation times were sufficiently short to avoid time dependent loss of or decrease in enzyme activity for ALDH1A1 or AOX. Protein and time linearity was confirmed for all systems employed. After the predefined incubation time, the reactions were terminated by adding an equal volume of ice-cold acetonitrile (ACN) with 20 nM *at*RA-d_5 (internal standard; IS). The samples were centrifuged at 15,000 *g* at 4℃ for 10 min and the supernatants were used for LC-MS/MS analysis. This method is referred to as *ACN precipitation method* in following sections. For incubations with low product formation, incubation volume was increased to 500 µL. After adding an equal volume of ice-cold ACN with 4 nM *at*RA-d_5 to stop the reaction, samples were processed using a *hexane extraction method*

(Arnold, Kent, Hogarth, and Isoherranen, 2015). In this method, each sample was extracted with 8 mL of hexanes, centrifuged at 1,000 *g* for 5 min, and the organic layer was transferred into a glass tube and dried under N_2 flow. The residue was resuspended with 100 µL of 80% ACN for LC-MS/MS analysis. Incubation time and concentrations of protein, substrate, inhibitor and cofactor used for incubations are specified for each experiment in the following sections. All incubations were performed under yellow light to prevent retinoid degradation and isomerization. All cofactor solutions were freshly prepared before incubations. As minor non-enzymatic formation of *at*RA was observed in incubations with retinaldehyde, incubations with no enzyme were included in each experiment and used for background subtraction. Unless described otherwise, all incubations were performed as duplicates or triplicates and repeated three times on separate days.

The formation of *at*RA in incubations was measured by LC-MS/MS with AB Sciex 5500 Q/LIT mass spectrometer (AB Sciex LLC, Framingham, MA) using positive ion APCI probe and equipped with an Agilent 1290 Infinity UHPLC (Agilent Technologies, Santa Clara, CA) and a Kinetex C18 column (1.7 µm, 100 Å, 2.1 x 100 mm; Phenomenex, Torrance, CA). The mobile phase consisted of H_2O with 0.1% formic acid (FA) (solvent A) and ACN with 0.1% FA (solvent B), respectively. The flow rate was 0.45 ml/min and the column temperature was set at 40°C. The gradient started at 50% B, increased to 95% B within 4.0 min and then was kept at 95% B for 1 min before returning to initial conditions. The injection volume was 20 µL per sample. *at*RA was monitored with multiple-reaction monitoring (MRM) transitions of *m/z* 301>205 and 301>123 and *at*RA-d_5 was monitored with *m/z* 306>208. All MS parameters were set as previously described (Arnold, Kent, Hogarth, and Isoherranen, 2015). Peaks of *at*RA and IS were integrated using Analyst 1.6.3. All *at*RA quantification methods followed best practices as previously reported for quantification of *at*RA (Czuba *et al.*, 2020). The peak area ratio of *at*RA to IS was used to quantify *at*RA formation. For quantification, standard curves of *at*RA (five concentrations ranging from 2 nM to 37.5 nM) were constructed by spiking *at*RA into KPi buffer and standard curve samples were processed in parallel with incubation samples. The ratio of *at*RA to *at*RA-d_5 (IS) peak area was plotted against *at*RA concentration (r^2 values >0.98 for all curves) and was used to calculate the concentration of *at*RA formed in incubations (Arnold, Kent, Hogarth, and Isoherranen, 2015). At least one representative experiment in replicates was analyzed by two different people in the lab to validate the analyses.

DMD Fast Forward. Published on December 18, 2020 as DOI: 10.1124/dmd.120.000296
This article has not been copyedited and formatted. The final version may differ from this version.

_at_RA formation by recombinant human AOX, ALDH1A1 and HLS9

To measure enzyme kinetic parameters of *at*RA formation from retinaldehyde with AOX, 10 nM recombinant AOX was incubated for 30 seconds with eleven concentrations of retinaldehyde ranging from 100 nM to 7.5 µM. Samples were processed with ACN precipitation method. Enzyme kinetic parameters, including k_{cat} and Michaelis-Menten constant (K_m), were obtained using GraphPad Prism5.0 (GraphPad Software, La Jolla, CA) by fitting Michaelis-Menten equation to the data. Enzyme kinetic parameters of *at*RA formation from retinaldehyde with recombinant human ALDH1A1 were measured as described previously (Arnold, Kent, Hogarth, and Isoherranen, 2015). To test cofactor dependence of *at*RA formation with HLS9, pooled HLS9 (0.02 µg protein μL^{-1}) were incubated with 2 µM retinaldehyde in the absence or presence of various cofactors. Tested cofactors and their final concentrations in incubations were 2 mM NAD^+, 2 mM $NADP^+$ and 1 mM NADPH. Incubation time was 30 seconds. Samples were processed with ACN precipitation method. To perform kinetic characterization of *at*RA formation with HLS9, pooled HLS9 (0.005 mg protein mL^{-1}) were incubated in the presence or absence of 2 mM NAD^+ for 40 seconds with various concentrations of retinaldehyde ranging from 10 nM to 10 µM. Samples were processed with the hexane extraction method. Enzyme kinetic parameters, including the maximum *at*RA formation velocity (V_{max}) and Michaelis-Menten constant in biological matrix (K_m), were obtained using GraphPad Prism 5.0 by fitting Michaelis-Menten equation to the data. As two enzymes were involved in *at*RA formation in HLS9 when NAD^+ was present, a two-enzyme Michaelis-Menten equation (equation 1) was fit to the data and to obtain kinetic parameters.

$$v = \frac{V_{max1}*[S]}{K_{m1}+[S]} + \frac{V_{max2}*[S]}{K_{m2}+[S]} \text{ (eq.1)}$$

In eq 1 K_m of enzyme 1 (K_{m1}) was constrained to be the value obtained from incubations performed without NAD^+ and V_{max1} constrained to be larger than 400 pmol min^{-1} mg S9 $protein^{-1}$. To build Eadie-Hofstee plots, *at*RA formation velocity (v) was plotted against v/[S] in which S is the substrate concentration.

Effects of CRBP1 on _at_RA formation by AOX and ALDH1A1

The effect of CRBP1 on *at*RA formation by AOX and ALDH1A1 was tested with recombinant proteins and pooled HLS9. CRBP-bound retinaldehyde (holo-CRBP)1 was prepared

DMD Fast Forward. Published on December 18, 2020 as DOI: 10.1124/dmd.120.000296
This article has not been copyedited and formatted. The final version may differ from this version.

by incubating 4 µM retinaldehyde for 5 min at room temperature with 4 µM CRBP1 in 100 mM KPi buffer, pH 7.4. The incubations were conducted with recombinant enzymes (5 nM AOX; 20 nM ALDH1A1) or pooled HLS9 (0.005 mg ml^{-1}) in 100 mM KPi buffer containing 2 mM NAD^+. The total incubation volume was 300 µL for recombinant enzymes and 1000 µL for pooled HLS9. Incubations were initiated by adding holo-CRBP1 (200 nM final concentration) or retinaldehyde (200 nM final concentration). The reaction was stopped by adding an equal volume of ice-cold ACN with 4 nM *at*RA-d_5. The incubation time was 1, 3 and 2 min for recombinant AOX, ALDH1A1 and HLS9, respectively. Samples were processed using the hexane extraction method and analyzed using LC-MS/MS.

Inhibition of *at*RA formation by AOX and ALDH1A1 inhibitors hydralazine, raloxifene and WIN18,446

Both hydralazine and raloxifene are known AOX inhibitors (Pryde *et al.*, 2010; Strelevitz *et al.*, 2012) while WIN18,446 is a selective ALDH1A inhibitor (Arnold, Kent, Hogarth, and Isoherranen, 2015). To build IC_{50} curves of hydralazine and raloxifene against AOX and to test whether WIN18,446 inhibits AOX activity, 10 nM recombinant human AOX was incubated with 0.5 µM retinaldehyde and 5-8 concentrations of raloxifene (1 nM - 5 µM), hydralazine (1 nM-100 µM) and WIN18,446 (1 µM-500 µM) for 2 minutes. All samples were processed with the ACN precipitation method. The IC_{50} values were determined by non-linear regression using GraphPad Prism 5.0 as described previously (Thatcher *et al.*, 2011).

To test whether hydralazine and raloxifene inhibit ALDH1A1 activity, 20 nM ALDH1A1 was incubated with 0.2 µM retinaldehyde, 2 mM NAD^+ and hydralazine (10 nM-1 mM) or raloxifene (1 nM-5 µM) in buffer containing 150 mM KCl and 50 mM Hepes-NaOH (pH 8.0). Incubations were initiated with the addition of NAD^+. The incubation time was 5 minutes. Control groups were incubations with no inhibitor. All samples were processed with ACN precipitation method. Percentage of control activity was calculated and plotted against inhibitor concentrations.

To determine the relative contribution to *at*RA formation by AOX and ALDH1A1 in human liver S9 fractions, pooled HLS9 and HLS9 from 3 individual liver donors (0.01 mg mL^{-1} $protein^{-1}$) were incubated with inhibitors and 0.2 µM retinaldehyde in the presence or absence of 2 mM NAD^+ for 30 sec. Tested inhibitors included WIN18,446 and hydralazine (final

DMD Fast Forward. Published on December 18, 2020 as DOI: 10.1124/dmd.120.000296
This article has not been copyedited and formatted. The final version may differ from this version.

concentration 250 μM). Control groups contained no inhibitor. Samples were processed with the hexane extraction method and the percentage of control activity was calculated. Incubations were also performed with 1 μM retinaldehyde as a substrate to test the impact of substrate concentration on enzyme contribution. Final concentrations of WIN18,446 and hydralazine were 500 μM in these experiments. Samples were processed with the ACN precipitation method.

Quantification of AOX and ALDH1A1 in HLS9 fractions using LC-MS/MS

AOX and ALDH1A1 protein concentrations in HLS9 were measured based on previously published protocols with minor modifications (Arnold *et al.*, 2016). Stable isotope labeled peptides (SIL) were ordered from Thermofisher Scientific (Waltham, MA) and used as IS for AOX and ALDH1A1 quantification (Table 1). SIL-peptides of AOX and ALDH1A1 were labeled with [$^{13}C_6{}^{15}N_2$] arginine and [$^{13}C_6{}^{15}N_2$] lysine, respectively.

Mouse liver S9 fractions were used as blank matrix (Arnold *et al.*, 2016) and diluted to 0.5 mg mL^{-1} with 100 mM ammonium bicarbonate buffer, pH 7.8. Various amounts of purified recombinant human AOX (0-4 pmol) and ALDH1A1 (0-10 pmol) were spiked into the diluted mouse liver S9 fractions (20 μL per sample) to make standard curve samples as described previously (Arnold *et al.*, 2016). HLS9 fractions (10 μg, 0.5 mg/mL) and standard curve samples were first incubated with 4 μL of 100 mM dithiothreitol and 10 μL of 100 mM ammonium bicarbonate buffer, pH 7.8 for 20 minutes at room temperature. After 5 μL of 10% sodium deoxycholate was added, samples were incubated at 95°C for 5 mins, then 4 μL of 200 mM iodoacetamide was added and the samples incubated at room temperature for 20 mins. The protein was digested with trypsin at 37°C for 15 hours at a 1:25 trypsin/protein (w/w) ratio. Trypsin digestion was stopped by the addition of 20 μL ice-cold ACN containing 8% trifluoroacetic acid and internal standards (50 nM SIL-peptide for AOX and 100 nM for ALDH1A1). Samples were centrifuged at 18,000 g at 4°C for 30 mins and supernatant was collected for LC-MS/MS analysis.

AOX and ALDH1A1 were quantified via measurement of the signature peptides (Table 1) using an AB Sciex 5500 QTrap Q-LIT mass spectrometer coupled with an Agilent 1290 HPLC and an Aeris peptide XB-C18 column (50 × 2.1 mm; 1.7 μm particle size). The MS parameters used are listed in Table 1. MS transitions for signature peptides of ALDH1A2 and 1A3 were also monitored. Other MS parameters and the LC conditions were as described

previously (Arnold *et al.*, 2016). The ratio of signature peptide peak area to SIL IS peptide area was used to construct standard curves and calculate AOX and ALDH1A1 concentrations in HLS9 fractions. The correlation between the protein expression levels and the *at*RA formation velocity was analyzed by first log-transforming the data and then testing the correlation via Pearson correlation. All measurements were performed in duplicates on three separate days.

Predictions of *at*RA formation velocity and intrinsic clearance of retinaldehyde in HLS9, and the relative contribution of AOX and ALDH1A1 to *at*RA formation

The intrinsic clearance (CL_{int}) of *at*RA formation from retinaldehyde was calculated using equation 2.

$$CL_{int} = \frac{V_{max}}{K_m} \quad \text{(eq.2)}$$

To scale the activity from the recombinant enzymes to HLS9, intersystem extrapolation factor (ISEF) was calculated using equation 3.

$$ISEF = \frac{CL_{int,pooled\ liver\ S9}}{CL_{int,recombinant}*[enzyme]} \quad \text{(eq.3)}$$

in which $CL_{int,\ pooled\ liver\ S9}$ is the measured intrinsic clearance in the pooled HLS9 sample and [enzyme] is the enzyme expression measured by LC-MS/MS in the pooled HLS9 sample. $ISEF_{AOX}$ is calculated with CL_{int} measured in the absence of NAD^+ while $ISEF_{ALDH1A1}$ is calculated with CL_{int} measured in the presence of NAD^+ minus the CL_{int} measured in the absence of NAD^+.

The *at*RA formation velocity in individual HLS9 samples was predicted based on the measured AOX and ALDH1A1 expression levels and the kinetics of *at*RA formation by recombinant enzymes using equation 4.

$$v_{enzyme} = \frac{ISEF*[enzyme]*k_{cat}*[S]}{K_m+[S]} \quad \text{(eq.4)}$$

in which v_{enzyme} is the predicted *at*RA formation velocity by a particular enzyme, [enzyme] is the enzyme expression measured in individual HLS9 samples prepared in this study, and [S] is the total substrate concentration. The average fold error (afe) of predictions of *at*RA formation velocity in three HLS9 samples from individual donors was calculated using equation 5.

$$\text{afe} = 10^{\frac{1}{n}\sum \log \frac{v_{predicted}}{v_{observed}}} \quad \text{(eq.5)}$$

DMD Fast Forward. Published on December 18, 2020 as DOI: 10.1124/dmd.120.000296
This article has not been copyedited and formatted. The final version may differ from this version.

in which $v_{predicted}$ and $v_{observed}$ are the predicted and observed *at*RA formation velocities of the individual HLS9 samples with 1 μM retinaldehyde as substrate. The afe values ranging from 0.5 to 1.5 were considered acceptable.

The predicted fraction metabolized by a particular enzyme (f_m) was calculated using equation 6:

$$f_{m,predicted} = \frac{v_{enzyme}}{v_{total}} \text{ (eq.6)}$$

in which v_{total} is the total *at*RA formation velocity ($v_{total}=v_{ALDH1A1}+v_{AOX}$) and v_{enzyme} is calculated from equation 4 in which [enzyme] is the average value of the enzyme expression measured in three HLS9 samples from individual donors.

The percent inhibition (%inhibition) of *at*RA formation in HLS9 caused by CRBP1 was predicted using equation 7.

$$\%inhibition = \%inhibition_{AOX} * f_{m,AOX} + \%inhibition_{ALDH1A1} * f_{m,ALDH1A1} \text{(eq.7)}$$

in which $\%inhibition_{enzyme}$ is the observed percent inhibition of the recombinant enzyme activity caused by CRBP1. Predicted f_m's by AOX and ALDH1A1 in the presence of CRBP1 ($cf_{m,enzyme}$) was calculated using equation 8.

$$cf_{m,enzyme} = \frac{\%inhibition_{enzyme} * f_{m,enzyme}}{\%inhibition_{AOX} * f_{m,AOX} + \%inhibition_{ALDH1A1} * f_{m,ALDH1A1}} \text{ (eq.8)}$$

In both equations 7 and 8, $f_{m,\ enzyme}$ indicates the observed relative contribution of a particular enzyme to *at*RA formation.

Results

Kinetics of *at*RA formation by AOX and ALDH1A1 and inhibition by raloxifene, hydralazine and WIN18,446

Recombinant human AOX oxidized retinaldehyde to yield *at*RA (Fig. 1A) with a K_m of 1.5 ± 0.4 μM and k_{cat} of 3.6 ± 2.0 min^{-1} (mean ± S.D., n=3), resulting in a CL_{int} of 2.6 ± 1.5 μL min^{-1} $pmol^{-1}$. In comparison, the K_m of retinaldehyde oxidation with ALDH1A1 was 0.25 μM and k_{cat} was 0.38 min^{-1} resulting in a CL_{int} of 1.5 μL min^{-1} $pmol^{-1}$ (Supplemental Figure 1). AOX inhibitors, raloxifene and hydralazine, both inhibited *at*RA formation by recombinant AOX with IC_{50} values <1 μM (Fig.1E and 1F). The IC_{50} value of hydralazine was about 3-fold higher than that of raloxifene (Table 2). WIN18,446 did not inhibit AOX activity at inhibitor concentrations

DMD Fast Forward. Published on December 18, 2020 as DOI: 10.1124/dmd.120.000296
This article has not been copyedited and formatted. The final version may differ from this version.

up to 500 µM while both AOX inhibitors, raloxifene and hydralazine, exhibited inhibitory effects on recombinant ALDH1A1 although at higher inhibitor concentrations than those causing AOX inhibition (Fig.1B-1D). Based on this data WIN18,446 is a selective inhibitor of ALDH1A1 at concentrations up to 100 µM. The difference in IC_{50} values between AOX and ALDH1A1 for raloxifene was only 10-fold suggesting raloxifene is not sufficiently selective as an inhibitor of AOX. In contrast, hydralazine can be used as a selective and potent inhibitor of AOX based on the >4,000-fold difference in the IC_{50} values between AOX and ALDH1A1 (Table 2).

_at_RA formation in HLS9

The potential enzymes forming *at*RA in human liver all use different cofactors, and therefore, cofactor dependence can be used to differentiate the enzyme contributions to *at*RA formation. In HLS9 *at*RA formation was observed in the absence of cofactors (NAD^+/$NADP^+$/NADPH; Fig. 2A), with a substrate concentration of 2 µM. Linear Eadie-Hofstee plot (Fig.2B) indicated that a single enzyme in HLS9 contributed to *at*RA formation in the absence of cofactors. V_{max} obtained by fitting the single enzyme Michaelis-Menten equation to the data was 646 ± 132 pmol min^{-1} mg^{-1} S9 protein and K_m of retinaldehyde was 1.4 ± 0.9 µM (mean ± S.D., n=3), similar to the K_m value measured with recombinant AOX. The CL_{int} for *at*RA formation was 615 ± 397 µL min^{-1} mg^{-1} S9 protein (mean ± S.D., n=3). Based on the fact that this activity did not require a cofactor, the enzyme responsible for this activity is likely AOX.

The addition of NADPH and NADH to the incubations did not result in any increase in *at*RA formation velocity in comparison to incubations without a cofactor, indicating that cytochrome P450 and NADH-dependent enzymes play a negligible role in retinaldehyde oxidation in human liver (Fig.2A). In the presence of NAD^+, the velocity of *at*RA formation measured with 2 µM retinaldehyde was about 1.8-fold higher than that measured in the absence of NAD^+. The Eadie-Hofstee plot (Fig.2C) indicated that two enzymes in HLS9 fractions were responsible for *at*RA synthesis in the presence of NAD^+. The low affinity enzyme was assumed to be AOX with the above described kinetic parameters. As the two-enzyme Michaelis-Menten model was fitted to the data, the high affinity enzyme V_{max} and K_m values were 518 ± 288 pmol min^{-1} mg^{-1} S9 protein and 0.38 ± 0.13 µM (mean ± S.D. n=3), respectively. The CL_{int} of the high affinity enzyme was 1,299 ± 370 µL min^{-1} mg^{-1} S9 protein (mean ± S.D., n=3) and the overall

DMD Fast Forward. Published on December 18, 2020 as DOI: 10.1124/dmd.120.000296
This article has not been copyedited and formatted. The final version may differ from this version.

CL_{int} was 1,914 µL min^{-1}mg S9 $protein^{-1}$. Based on the requirement of NAD^+ for the activity of the observed second enzyme, this activity is likely ALDH1A1. Taken together, these data strongly support that both ALDH1A1 and AOX contribute to *at*RA biosynthesis in human liver.

Predicted contribution of AOX and ALDH1A1 to *at*RA formation in HLS9

The signature peptide of AOX for quantification was selected based on the MS signal intensity and peptide stability in matrix (Supplemental Figure 2). The selected human AOX and ALDH1A1 quantification peptides were observed in HLS9 but not in mouse liver S9 demonstrating the specificity of these peptides (Fig.3A and 3B). The expression level of ALDH1A1 in HLS9 (156-285 pmol mg S9 $protein^{-1}$) was on average 13- fold higher than the expression of AOX (9.4 -24 pmol mg S9 $protein^{-1}$) (Fig.3C). No expression of ALDH1A2 or ALDH1A3 was detected in the HLS9 (data not shown).

Using CL_{int} obtained in the pooled HLS9 and recombinant enzymes, $ISEF_{AOX}$ and $ISEF_{ALDH1A1}$ were calculated to be 25 and 6, respectively. The predicted velocity of *at*RA formation mediated by AOX in the three individual livers ranged from 586 to 846 pmol $min^{-1}mg^{-1}$ S9 while the predicted total velocity including AOX and ALDH1A1 ranged from 943 to 1,366 pmol $min^{-1}mg^{-1}$ S9. When compared to the observed formation velocities in the three individual livers, AOX mediated formation of *at*RA had an afe of 1.35 while the total velocity had an afe of 0.71, both within two-fold of the observed velocities measured without (371-655 pmol $min^{-1}mg^{-1}$ S9) and with (1,377-1,861 pmol $min^{-1}mg^{-1}$ S9; Fig.3) NAD^+. With NAD^+, *at*RA formation velocity measured with 1 µM retinaldehyde positively correlated with the enzyme expression of ALDH1A1 (r=0.99; p=0.011) and AOX (r=0.98; p=0.022) in HLS9 (Fig.3D and 3E). However, the AOX expression did not show a correlation with *at*RA formation velocity measured in the absence of NAD^+ (r=-0.80; p=0.20; Fig.3E) possibly suggesting that not all MS quantified AOX in the liver is catalytically active (Fu *et al.*, 2013). The expression of ALDH1A1 showed a weak correlation with the expression of AOX (r=0.94; p=0.065).

The fraction of *at*RA formation by AOX and ALDH1A1 (f_m) is expected to vary with retinaldehyde concentration due to the differences in the K_m values for the two enzymes. Based on the AOX and ALDH1A1 expression and *at*RA formation kinetics, the $f_{m,AOX}$ was predicted to increase from 0.36 to 0.73 while $f_{m,ALDH1A1}$ was predicted to decrease from 0.64 to 0.27 as retinaldehyde concentration increased from low nM concentrations to saturating concentrations

DMD Fast Forward. Published on December 18, 2020 as DOI: 10.1124/dmd.120.000296
This article has not been copyedited and formatted. The final version may differ from this version.

(5 µM) (Fig.3F). As such, determination of relative importance of each enzyme to *at*RA formation in human liver depends on substrate concentrations and should be assessed at biologically relevant concentrations of retinaldehyde.

Observed relative contribution of AOX and ALDH1A1 to *at*RA formation in HLS9

To determine the quantitative contributions of ALDH1A1 and AOX to *at*RA formation in human livers, inhibition of *at*RA formation in human liver by hydralazine (selective AOX inhibitor) and WIN18,446 (selective ALDH1A1 inhibitor) was characterized. Inhibitor concentrations used in HLS9 incubations were first tested with purified recombinant enzymes to confirm selectivity and efficacy of inhibition. At their selected concentrations, hydralazine and WIN18,446 caused >95% inhibition of their target enzymes, AOX and ALDH1A1, without inhibiting the non-targeted enzymes (Fig.4A and 4B). In HLS9 incubations without NAD^+ cofactor, hydralazine inhibited >95% of *at*RA formation while WIN18,446 did not lead to any significant inhibition. This data confirms that AOX is the enzyme responsible for the non-NAD^+ dependent formation of *at*RA. In the presence of NAD^+, hydralazine inhibited only 24 ± 6 % (mean ± S.D., n=4) of *at*RA formation in HLS9 with a substrate concentration of 0.2 µM while WIN18,446 inhibited 81 ± 6 % (mean ± S.D., n=4) of *at*RA formation (Fig.4C and 4D). The predicted f_m of ALDH1A1 (0.53) underpredicted ALDH1A1 contribution to *at*RA formation in HLS9 at 0.2 µM retinaldehyde while that of AOX (0.47) was overestimated (Fig.3F). With 1 µM retinaldehyde as a substrate, hydralazine and WIN 18,446 inhibited 47 ± 15% and 56 ± 11% (mean ± S.D., n=4) of the total *at*RA formation activity, respectively, demonstrating the decreased contribution of ALDH1A1 to *at*RA formation at higher substrate concentrations (Fig.4E and4F). The observed % inhibition at 1 µM retinaldehyde was higher than the predicted f_m of ALDH1A1 (0.38) and lower than the predicted f_m of AOX (0.62) (Fig.3F). The combination of hydralazine and WIN18,446 abolished >95% of *at*RA formation in HLS9 samples when incubated in the presence of NAD^+ suggesting that AOX and ALDH1A1 are the only enzymes contributing to *at*RA formation in HLS9.

Effects of CRBP1 on AOX and ALDH1A1 activity

To determine whether binding to CRBP1 affects the formation of *at*RA by AOX or ALDH1A1 and their relative importance in hepatic *at*RA formation, *at*RA formation velocity

was measured with recombinant enzymes and HLS9 using holo-CRBP1 as the substrate. As shown in Figure 5A, in the presence of CRBP1 the formation of *at*RA by AOX and ALDH1A1 decreased about 85 and 55% in comparison to control incubations that contained no CRBP1. As AOX and ALDH1A1 contribute about 20 and 80% to *at*RA formation in HLS9 in the absence of CRBP1, the activity of *at*RA formation in HLS9 was predicted to decrease by 61% in the presence of CRBP1. The f_ms by AOX and ALDH1A1 were estimated to be 0.08 and 0.92, respectively, in the presence of CRBP1 (Fig.5B). The decrease in *at*RA formation caused by CRBP1 was tested in HLS9, and the addition of CRBP1 decreased *at*RA formation by 63% when compared to the no CRBP control (Fig.5A), a level of inhibition consistent with predictions.

Discussion

To date, majority of the knowledge regarding the role of specific *at*RA biosynthesis enzymes is derived from studies in developmental biology and altered retinoid signaling during embryonic development. Yet, the biological importance of vitamin A metabolizing enzymes defined during embryonic development does not always translate to postnatal life. For example, the embryonic knockout of Aldh1a2 leads to embryonic death in mice (Niederreither *et al.*, 2002), but neither tamoxifen-induced postnatal global knockout of Aldh1a2 or germ-cell specific deletion of Aldh1a2 caused any abnormal phenotype (Beedle *et al.*, 2019). A similar discrepancy was observed with *at*RA hydroxylase Cyp26a1. Cyp26a1 knockout is embryonic lethal, but postnatal knockout has no major effects on mouse health (Zhong, Hogarth, *et al.*, 2019). While knockout mouse models have allowed considerable progress in defining the enzymology of vitamin A and retinoid homeostasis, knowledge of the role of specific enzymes in *at*RA biosynthesis in human tissues is still limited. This includes limited knowledge of the identity of the enzymes synthesizing *at*RA in the human liver, the main storage organ for vitamin A. The goal of this study was to determine the main enzymes synthesizing *at*RA in the human liver and test the hypothesis that AOX contributes to *at*RA biosynthesis in the human liver.

This study unequivocally shows that AOX forms *at*RA from retinaldehyde and that in human liver ALDH1A1 and AOX contribute to *at*RA biosynthesis. Recombinant AOX exhibited about 6-fold higher K_m and 1.6-fold higher CL_{int} than ALDH1A1 for *at*RA formation, showing that ALDH1A1 is a high affinity-low capacity *at*RA synthesizing enzyme while AOX is a low affinity -high capacity enzyme. According to the human protein ATLAS database, AOX protein

DMD Fast Forward. Published on December 18, 2020 as DOI: 10.1124/dmd.120.000296
This article has not been copyedited and formatted. The final version may differ from this version.

is expressed in the kidney, bladder, pancreas, endocrine tissues and reproductive tissues (https://www.proteinatlas.org/ENSG00000138356-AOX1/tissue). This suggests that AOX may contribute to *at*RA synthesis in the testis among other tissues. However, studies in healthy mice have shown that AOX activity is not quantitatively significant in the mouse testis (Arnold, Kent, Hogarth, Griswold, *et al.*, 2015), but rather that AOX plays a role in testicular *at*RA synthesis in mice when ALDH1A activity is impaired (Beedle *et al.*, 2019). This is in agreement with the findings in the human testis showing that ALDH1A1 and ALDH1A2 are responsible for >95% of *at*RA formation in this tissue (Arnold, Kent, Hogarth, and Isoherranen, 2015). In contrast to the testis, AOX appears to contribute about 50% of *at*RA biosynthesis in mouse liver (Arnold, Kent, Hogarth, Griswold, *et al.*, 2015). This suggests a tissue specific role of AOX that likely depends on the expression levels of AOX and the complement of ALDH1A enzymes expressed in the different tissues. The results of this study support a similar role of AOX in *at*RA biosynthesis in human liver as in the mouse liver, with AOX contributing between 33 and 70% of *at*RA biosynthesis depending on retinaldehyde concentration. The reported total concentrations of retinaldehyde in the liver and adipose are 100-200 pmol/g (~150 nM) (Ziouzenkova *et al.*, 2007; Kane *et al.*, 2008). These concentrations are much below the K_m towards AOX (1.5 µM) but similar to the K_m towards ALDH1A1 (0.25 µM). Due to the difference in K_m-values for AOX and ALDH1A1, the predicted and observed f_m of retinaldehyde by AOX show a clear dependence on retinaldehyde concentration within the evaluated range of 20-2000 nM retinaldehyde. As the concentration of retinaldehyde increases, $f_{m,AOX}$ increases due to the saturation of the high affinity ALDH1A1. This also suggests that in the case of ALDH1A dysfunction (inhibition, downregulation or genetic defect) or excess retinoid/vitamin A (saturation of ALDH1A1), AOX plays an important role in regulating hepatic vitamin A homeostasis. The relative contribution of AOX (30-70%) to *at*RA biosynthesis is supported by the scaling of *at*RA formation from recombinant enzymes, the quantification of AOX and ALDH1A1 protein expression in the liver, the cofactor dependence of *at*RA formation, and the inhibition of *at*RA formation by selective ALDH1A and AOX inhibitors WIN18,446 and hydralazine. These tools developed in the current study allow differentiation of ALDH1A and AOX contributions to *at*RA formation and can be further applied to other critical retinoid responsive tissues such as the skin, hematopoietic cells and adipose tissue, to determine the enzymes contributing to *at*RA biosynthesis. Such information will be useful in predicting how

inhibition of genetic variability in AOX and ALDH1A enzymes will affect retinoid homeostasis and signaling.

In tissues that contribute to vitamin A homeostasis, CRBP1 is expressed and retinoids are believed to be bound to retinoid binding proteins (Noy, 2000; Napoli, 2016). As such CRBP1 can impact retinoid metabolism and the enzymology of *at*RA biosynthesis. The presence of CRBP1 decreased the *at*RA formation velocity by both ALDH1A1 and AOX. This finding is in agreement with previous demonstration that with CRBP1 the activity of ALDH1A1 mediated *at*RA formation decreased about 52% when compared to the activity measured without CRBP1 (Arnold, Kent, Hogarth, and Isoherranen, 2015). Similarly, with 0.2 μM CRBP1-bound retinaldehyde as a substrate, *at*RA formation velocity measured in the E2 fraction (associated with AOX) from soluble extracts of human liver was about 70-80% lower than that measured without CRBP1 (Ambroziak *et al.*, 1999). However, as shown here, CRBP1 binding decreased *at*RA formation by both ALDH1A1 and AOX, and therefore the impact of CRBP1 on the f_m's by AOX and ALDH1A1 is likely modest. In addition, CRBP1 binding is unlikely to have a significant impact on *at*RA formation in vivo as CRABP1 in human liver is expected to be bound by hepatic retinol (1.2-162 μM; (Zhong, Kirkwood, *et al.*, 2019)) which has a K_d of ~18.6 nM to CRBP1 compared to K_d of retinaldehyde ~44nM; (Ambroziak *et al.*, 1999; Silvaroli *et al.*, 2016).

The results of this study show that the human liver possesses a high *at*RA biosynthesis capacity. The observed *at*RA formation velocity in the HLS9 observed here (1,043-1,861 pmol $min^{-1}mg^{-1}$ S9 protein) is 31 to 56-fold higher than the observed *at*RA formation velocity in human testis (33.3 pmol $min^{-1}mg^{-1}$ S10 protein at 1 μM retinaldehyde) (Arnold, Kent, Hogarth, and Isoherranen, 2015). This difference in *at*RA formation velocities is comparable to the difference between human testicular (4.3 ± 0.5 pmol g^{-1} testis) and hepatic tissue *at*RA concentrations (14-580 pmol g^{-1}, median 43 pmol g^{-1} liver) (Arnold, Kent, Hogarth, and Isoherranen, 2015; Zhong, Kirkwood, *et al.*, 2019). This finding supports the previous report in human testis that variability in tissue *at*RA formation kinetics could be used to predict the variability in tissue *at*RA concentrations (Arnold, Kent, Hogarth, and Isoherranen, 2015). The velocity of *at*RA formation in HLS9 was successfully predicted at a single concentration of retinaldehyde in this study when AOX and ALDH1A1 protein expression and specific ISEF values were applied to individual donors. As reported in the literature, with xenobiotic substrates

of AOX, AOX activity is often poorly scaled from one system to another (e.g. recombinant enzyme to cytosol, in vitro to in vivo) and recombinant AOX typically underpredicts the activity in native environment (Pryde *et al.*, 2010; Fu *et al.*, 2013) suggesting that *at*RA biosynthesis may be more efficient by AOX in vivo than predicted from the HLS9 here. This finding was confirmed in the current study with the data suggesting an ISEF value of 20 for AOX. Surprisingly, ALDH1A1 also had an ISEF value of 6 in this study when previous work in the human testis indicated an ISEF value of approximately 2 for ALDH1A. As ISEF values may vary for different tissues and for different enzymes, these findings emphasize the importance of independent experiments such as selective inhibition studies to determine the relative contributions of individual enzymes to *at*RA formation.

In conclusion, this study shows that human AOX is responsible for 30-70% of *at*RA biosynthesis in human liver. The importance of AOX and ALDH1A1 in *at*RA biosynthesis and in regulation of *at*RA signaling is an intriguing intersection between xenobiotic and endogenous compound metabolism. As many AOX inhibitors are therapeutic drugs, the administration of these drugs may affect *at*RA gradients and signaling in the liver and other tissues. Determining whether AOX inhibition in the liver or in other organs alters *at*RA concentrations and biosynthesis requires further study. Additionally, reported single nucleotide polymorphisms of human AOX (Hartmann *et al.*, 2012; Hutzler *et al.*, 2014; Foti *et al.*, 2017) may have an impact on in vivo retinaldehyde clearance and tissue *at*RA gradients. As such the impact of altered AOX activity on *at*RA concentrations and vitamin A homeostasis should be considered in preclinical and clinical studies.

Acknowledgments

Authorship contributions

Participated in research design: Zhong, Isoherranen.

Conducted experiments: Zhong, Seaman, Xi, Paragas, Herpoldt.

Contributed new reagents or analytic tools: Paragas, Jones, Herpoldt, King.

Performed data analysis: Zhong, Seaman.

Wrote or contributed to the writing of the manuscript: Zhong, Seaman, Paragas, Herpoldt, King, Jones, Isoherranen.

References

Ambroziak W, Izaguirre G, and Pietruszko R (1999) Metabolism of Retinaldehyde and Other Aldehydes in Soluble Extracts of Human Liver and Kidney. *J Biol Chem* **274**:33366–33373.

Arnold SL, Kent T, Hogarth CA, Griswold MD, Amory JK, and Isoherranen N (2015) Pharmacological inhibition of ALDH1A in mice decreases all-trans retinoic acid concentrations in a tissue specific manner. *Biochem Pharmacol* **95**:177–192.

Arnold SL, Kent T, Hogarth CA, and Isoherranen N (2015) Importance of ALDH1A enzymes in determining human testicular retinoic acid concentrations. *J Lipid Res* **56**:342–357.

Arnold SL, Stevison F, and Isoherranen N (2016) Impact of Sample Matrix on Accuracy of Peptide Quantification: Assessment of Calibrator and Internal Standard Selection and Method Validation. *Anal Chem* **88**:746–753.

Barr JT, Jones JP, Joswig-Jones CA, and Rock DA (2013) Absolute Quantification of Aldehyde Oxidase Protein in Human Liver Using Liquid Chromatography–Tandem Mass Spectrometry. *Mol Pharm* **10**:3842–3849.

Beedle MT, Stevison F, Zhong G, Topping T, Hogarth C, Isoherranen N, and Griswold MD (2019) Sources of all-trans retinal oxidation independent of the aldehyde dehydrogenase 1A isozymes exist in the postnatal testis. *Biol Reprod* **100**:547–560.

Czuba LC, Zhong G, Yabut KC, and Isoherranen N (2020) Analysis of vitamin A and retinoids in biological matrices. *Methods Enzymol* **637**:309–340.

Fan X, Molotkov A, Manabe S-I, Donmoyer CM, Deltour L, Foglio MH, Cuenca AE, Blaner WS, Lipton SA, and Duester G (2003) Targeted Disruption of Aldh1a1 (Raldh1) Provides Evidence for a Complex Mechanism of Retinoic Acid Synthesis in the Developing Retina. *Mol Cell Biol* **23**:4637–4648.

Foti A, Dorendorf F, and Leimkühler S (2017) A single nucleotide polymorphism causes enhanced radical oxygen species production by human aldehyde oxidase. *PLoS One* **12**:e0182061.

Fu C, Di L, Han X, Soderstrom C, Snyder M, Troutman MD, Obach RS, and Zhang H (2013) Aldehyde Oxidase 1 (AOX1) in Human Liver Cytosols: Quantitative Characterization of AOX1 Expression Level and Activity Relationship. *Drug Metab Dispos* **41**:1797–1804.

Hartmann T, Terao M, Garattini E, Teutloff C, Alfaro JF, Jones JP, and Leimkühler S (2012) The Impact of Single Nucleotide Polymorphisms on Human Aldehyde Oxidase. *Drug*

Metab Dispos **40**:856–864.

Huang D-Y, Furukawa A, and Ichikawa Y (1999) Molecular Cloning of Retinal Oxidase/Aldehyde Oxidase cDNAs from Rabbit and Mouse Livers and Functional Expression of Recombinant Mouse Retinal Oxidase cDNA inEscherichia coli. *Arch Biochem Biophys* **364**:264–272.

Hutzler JM, Yang Y-S, Brown C, Heyward S, and Moeller T (2014) Aldehyde Oxidase Activity in Donor-Matched Fresh and Cryopreserved Human Hepatocytes and Assessment of Variability in 75 Donors. *Drug Metab Dispos* **42**:1090–1097.

Kane MA, Folias AE, and Napoli JL (2008) HPLC/UV quantitation of retinal, retinol, and retinyl esters in serum and tissues. *Anal Biochem* **378**:71–79.

Kedishvili NY (2013) Enzymology of retinoic acid biosynthesis and degradation. *J Lipid Res* **54**:1744–1760.

Napoli JL (2016) Functions of Intracellular Retinoid Binding-Proteins. *Subcell Biochem* **81**:127–161.

Napoli JL (2012) Physiological insights into all-trans-retinoic acid biosynthesis. *Biochim Biophys Acta - Mol Cell Biol Lipids* **1821**:152–167, Elsevier B.V.

Niederreither K, Vermot J, Schuhbaur B, Chambon P, and Dollé P (2002) Embryonic retinoic acid synthesis is required for forelimb growth and anteroposterior patterning in the mouse. *Development* **129**:3563–3574.

Noy N (2000) Retinoid-binding proteins: Mediators of retinoid action. *Biochem J* **348**:481–495.

Paragas EM, Humphreys SC, Min J, Joswig-Jones CA, Leimkühler S, and Jones JP (2017) ecoAO: A Simple System for the Study of Human Aldehyde Oxidases Role in Drug Metabolism. *ACS Omega* **2**:4820–4827.

Pryde DC, Dalvie D, Hu Q, Jones P, Obach RS, and Tran TD (2010) Aldehyde oxidase: An enzyme of emerging importance in drug discovery. *J Med Chem* **53**:8441–8460.

Rashidi M-RR, and Soltani S (2017) An overview of aldehyde oxidase: an enzyme of emerging importance in novel drug discovery. *Expert Opin Drug Discov* **12**:305–316.

Silvaroli JA, Arne JM, Chelstowska S, Kiser PD, Banerjee S, and Golczak M (2016) Ligand Binding Induces Conformational Changes in Human Cellular Retinol-binding Protein 1 (CRBP1) Revealed by Atomic Resolution Crystal Structures. *J Biol Chem* **291**:8528–8540.

Strelevitz TJ, Orozco CC, and Obach RS (2012) Hydralazine as a selective probe inactivator of

aldehyde oxidase in human hepatocytes: Estimation of the contribution of aldehyde oxidase to metabolic clearance. *Drug Metab Dispos* **40**:1441–1448.

Terao M, Garattini E, Romão MJ, and Leimkühler S (2020) Evolution, expression, and substrate specificities of aldehyde oxidase enzymes in eukaryotes. *J Biol Chem* **295**:5377–5389.

Terao M, Kurosaki M, Barzago MM, Fratelli M, Bagnati R, Bastone A, Giudice C, Scanziani E, Mancuso A, Tiveron C, and Garattini E (2009) Role of the molybdoflavoenzyme aldehyde oxidase homolog 2 in the biosynthesis of retinoic acid: generation and characterization of a knockout mouse. *Mol Cell Biol* **29**:357–77.

Thatcher JE, Buttrick B, Shaffer SA, Shimshoni JA, Goodlett DR, Nelson WL, and Isoherranen N (2011) Substrate specificity and ligand interactions of CYP26A1, the human liver retinoic acid hydroxylase. *Mol Pharmacol* **80**:228–39.

Tomita S, Tsujita M, and Ichikawa Y (1993) Retinal oxidase is identical to aldehyde oxidase. *FEBS Lett* **336**:272–274.

Zhong G, Hogarth C, Snyder JM, Palau L, Topping T, Huang W, Czuba LC, LaFrance J, Ghiaur G, and Isoherranen N (2019) The retinoic acid hydroxylase Cyp26a1 has minor effects on postnatal Vitamin A homeostasis, but is required for exogenous atRA clearance. *J Biol Chem*, doi: 10.1074/jbc.RA119.009023.

Zhong G, Kirkwood J, Won K-J, Tjota N, Jeong H, and Isoherranen N (2019) Characterization of Vitamin A Metabolome in Human Livers With and Without Nonalcoholic Fatty Liver Disease. *J Pharmacol Exp Ther* **370**:92–103.

Ziouzenkova O, Orasanu G, Sharlach M, Akiyama TE, Berger JP, Viereck J, Hamilton JA, Tang G, Dolnikowski GG, Vogel S, Duester G, and Plutzky J (2007) Retinaldehyde represses adipogenesis and diet-induced obesity. *Nat Med* **13**:695–702.

Footnotes

This study was supported by the National Institutes of Health [Grant R01 GM111772].

Legends for figures

Figure 1. Characterization of *at*RA formation by recombinant human AOX, and inhibition of AOX and ALDH1A1 mediated *at*RA formation by raloxifene, hydralazine and WIN18,446. Panel A shows a representative Michaelis-Menten plot of *at*RA formation with recombinant AOX. Panels B and C show the inhibition of recombinant ALDH1A1 mediated *at*RA formation by raloxifene (B) and hydralazine (C). Panels D-F show the inhibition of recombinant AOX mediated *at*RA formation by WIN18,446 (D), raloxifene (E) and hydralazine (F). For determination of IC_{50} values the bottom and the top of IC_{50} curves were constrained to be > 0 and < 120, respectively. Each panel shows a representative plot obtained from one of the three experiments performed on separate days. Data points and error bars represent mean and S.D. of triplicates within the experiment.

Figure 2. Characterization of *at*RA formation in human liver. Panel A shows the dependence of *at*RA formation on different cofactors in pooled HLS9. Each data point represents one of three assays performed on separate days. Horizontal lines and error bars represent mean and S.D. of the measurements over the different days. The retinaldehyde concentration used in the incubations was 2 μM. Non-enzymatic *at*RA formation was subtracted from the total *at*RA formation to calculate the velocity of enzymatic *at*RA formation in each group. Panels B and C show retinaldehyde concentration dependent *at*RA formation by HLS9 in the absence (B) and presence (C) of NAD^+. Representative Eadie-Hofstee plots of *at*RA formation by HLS9 are shown with the Michaelis-Menten plots of *at*RA formation shown in insets. Each Eadie-Hofstee plot is a representative plot obtained from one of the three experiments performed on separate days. Data points and error bars represent mean and S.D. of triplicates within the day. The inset in panel B shows the fit of a single-enzyme Michaelis-Menten equation to the data while the inset in panel C shows the fit of a two-enzyme Michaelis-Menten equation to the data as described in Materials and Methods.

Figure 3. Characterization of expression of AOX and ALDH1A1 and their predicted contribution to *at*RA formation in human liver. Panels A and B show the LC-MS/MS measurement of AOX and ALDH1A1 protein expression. The quantified MS/MS transitions of AOX (*m/z* 605.3>963.5) and ALDH1A1 (*m/z* 795.4 > 879.5) signature peptides are shown in black and

orange, respectively. Panel A shows the LC-MS/MS chromatogram of a sample of mouse liver S9 (MLS9) fraction spiked with 1 pmol purified recombinant human AOX and 2.5 pmol purified recombinant human ALDH1A1 (standard sample). The inset in panel A shows MLS9 without adding any recombinant human AOX and ALDH1A1. Panel B shows a representative chromatogram of pooled human liver S9 fraction and detection of AOX and ALDH1A1 in human liver. Panel C shows the correlation between AOX and ALDH1A1 protein expression, and panels D and E show the correlation between the ALDH1A1 (D) and AOX (E) protein expression and the observed *at*RA formation velocity measured at 1μM retinaldehyde. "Activity (NAD^+)" indicates the total velocity measured in the presence of NAD^+ that reflects contribution by both AOX and ALDH1A1; "Activity (No NAD^+)" indicates the velocity measured in the absence of NAD^+ reflecting only AOX activity; Activity (NAD^+-No NAD^+) = Activity (NAD^+) - Activity (No NAD^+). Each symbol represents an individual HLS9 sample. Symbols represent the mean values of three individual experiments conducted on separate days in duplicates. The dash lines show the linear regression between the enzyme expression and *at*RA formation velocity; *p* values shown in the panels indicate whether the slope of the corresponding line is significantly different from zero. Panel F shows the dependence of predicted ALDH1A1 and AOX contributions to *at*RA formation (f_m) on retinaldehyde concentrations. The solid lines indicate predicted f_m of *at*RA formation by ALDH1A1 (orange) and AOX (black) in HLS9 fractions.

Figure 4. Effect of selective AOX and ALDH1A1 inhibitors on *at*RA formation by recombinant enzymes and human liver S9 fractions. Retinaldehyde concentrations used in incubations were 0.2 (left column) and 1 μM (right column) while inhibitor concentrations (HDZ and WIN) were 250 μM in left panels and 500 μM in right panels. In panels A and B, inhibition assays were performed using recombinant human ALDH1A (open triangles) and AOX (open circles). In panels C-F, inhibition assays were done using HLS9 fractions and panels C and D show incubations in the absence of NAD^+ while E and F show incubations in the presence of NAD^+. Bars represent mean values of three individual experiments performed on separate days while each data point represent an individual experiment done in duplicates. Different bars and symbols represent pooled HLS9 (filled gray bars) and HLS9 fractions from three individual donors (dashed, white and dotted bars). HDZ, hydralazine; WIN, WIN18,446.

Figure 5. Effects of CRBP1 on *at*RA formation by recombinant AOX, ALDH1A1 and human liver S9. Panel A shows *at*RA formation velocity when free retinaldehyde (-CRBP) or holo-CRBP1 (+CRABP) is used as a substrate. The bars represent the mean % inhibition from three individual experiments conducted on separate days and error bars represent S.D.. Panel B shows the predicted fraction of retinaldehyde metabolized by AOX and ALDH1A1 in the presence and absence of CRBP1. The substrate concentration (retinaldehyde or CRBP1-bound retinaldehyde) was 0.2 μM in all experiments.

DMD Fast Forward. Published on December 18, 2020 as DOI: 10.1124/dmd.120.000296
This article has not been copyedited and formatted. The final version may differ from this version.

Tables

Table 1. Peptide sequences and MS parameters for AOX and ALDH1A signature peptides selected for protein quantification using LC-MS/MS.

	peptide	Precursor ion (m/z)	Fragment ion (m/z)	DP (V)	CE (V)
AOX	VFFGEGDGIIR	605.3	963.5, 816.4	80	17
	VFFGEGDGII**R**	610.3	973.5, 826.4	80	17
ALDH1A1	ANNTFYGLSAGVFTK	795.4	1042.6, 879.5	120	20
	ANNTFYGLSAGVFT**K**	799.4	1050.6, 887.5	120	20
ALDH1A2	ILELIQSGVAEGAK	714.4	846.4, 959.5	120	30
ALDH1A3	EEIFGPVQPILK	685.4	851.5, 794.5	81	34

Note: DP, declustering potential; CE, collision energy.

Labeled amino acids in the SIL-peptides are shown as bolded letters. SIL-peptides of AOX and ALDH1A1 were labeled with [$^{13}C_6{}^{15}N_2$] arginine and [$^{13}C_6{}^{15}N_2$] lysine, respectively. ALDH1A2 and ALDH1A3 were not detected in any HLS9 samples used in this study.

Table 2. IC_{50} values of raloxifene, hydralazine and WIN18,446 measured against recombinant AOX and ALDH1A1 enzymes (mean ± S.D., n=3)

	AOX	ALDH1A1	Selectivity index
Raloxifene (μM)	0.15 ± 0.05	1.54 ± 0.54	10.3
Hydralazine (μM)	0.42 ± 0.21	1840 ± 690	4381
WIN18,446 (μM)	>500	0.102[a]	>4900

a, the IC_{50} value is from Arnold et al., 2015

The selectivity index was calculated by dividing the IC_{50} value of the non-target enzyme by the IC_{50} value of the target enzyme.

Figures

Figure 1. Characterization of *at*RA formation by recombinant human AOX, and inhibition of AOX and ALDH1A1 mediated *at*RA formation by raloxifene, hydralazine and WIN18,446. Panel A shows a representative Michaelis-Menten plot of *at*RA formation with recombinant AOX. Panels B and C show the inhibition of recombinant ALDH1A1 mediated *at*RA formation by raloxifene (B) and hydralazine (C). Panels D-F show the inhibition of recombinant AOX mediated *at*RA formation by WIN18,446 (D), raloxifene (E) and hydralazine (F). For determination of IC_{50} values the bottom and the top of IC_{50} curves were constrained to be > 0 and < 120, respectively. Each panel shows a representative plot obtained from one of the three experiments performed on separate days. Data points and error bars represent mean and S.D. of triplicates within the experiment.

Figure 2. Characterization of *at*RA formation in human liver. Panel A shows the dependence of *at*RA formation on different cofactors in pooled HLS9. Each data point represents one of three assays performed on separate days. Horizontal lines and error bars represent mean and S.D. of the measurements over the different days. The retinaldehyde concentration used in the incubations was 2 μM. Non-enzymatic *at*RA formation was subtracted from the total *at*RA formation to calculate the velocity of enzymatic *at*RA formation in each group. Panels B and C show retinaldehyde concentration dependent *at*RA formation by HLS9 in the absence (B) and presence (C) of NAD^+. Representative Eadie-Hofstee plots of *at*RA formation by HLS9 are shown with the Michaelis-Menten plots of *at*RA formation shown in insets. Each Eadie-Hofstee plot is a representative plot obtained from one of the three experiments performed on separate days. Data points and error bars represent mean and S.D. of triplicates within the day. The inset in panel B shows the fit of a single-enzyme Michaelis-Menten equation to the data while the inset in panel C shows the fit of a two-enzyme Michaelis-Menten equation to the data as described in Materials and Methods.

Figure 3. Characterization of expression of AOX and ALDH1A1 and their predicted contribution to *at*RA formation in human liver. Panels A and B show the LC-MS/MS measurement of AOX and ALDH1A1 protein expression. The quantified MS/MS transitions of AOX (*m/z*

605.3>963.5) and ALDH1A1 (*m/z* 795.4 > 879.5) signature peptides are shown in black and orange, respectively. Panel A shows the LC-MS/MS chromatogram of a sample of mouse liver S9 (MLS9) fraction spiked with 1 pmol purified recombinant human AOX and 2.5 pmol purified recombinant human ALDH1A1 (standard sample). The inset in panel A shows MLS9 without adding any recombinant human AOX and ALDH1A1. Panel B shows a representative chromatogram of pooled human liver S9 fraction and detection of AOX and ALDH1A1 in human liver. Panel C shows the correlation between AOX and ALDH1A1 protein expression, and panels D and E show the correlation between the ALDH1A1 (D) and AOX (E) protein expression and the observed *at*RA formation velocity measured at 1μM retinaldehyde. "Activity (NAD^+)" indicates the total velocity measured in the presence of NAD^+ that reflects contribution by both AOX and ALDH1A1; "Activity (No NAD^+)" indicates the velocity measured in the absence of NAD^+ reflecting only AOX activity; Activity (NAD^+-No NAD^+) = Activity (NAD^+) - Activity (No NAD^+). Each symbol represents an individual HLS9 sample. Symbols represent the mean values of three individual experiments conducted on separate days in duplicates. The dash lines show the linear regression between the enzyme expression and *at*RA formation velocity; *p* values shown in the panels indicate whether the slope of the corresponding line is significantly different from zero. Panel F shows the dependence of predicted ALDH1A1 and AOX contributions to *at*RA formation (f_m) on retinaldehyde concentrations. The solid lines indicate predicted f_m of *at*RA formation by ALDH1A1 (orange) and AOX (black) in HLS9 fractions.

Figure 4. Effect of selective AOX and ALDH1A1 inhibitors on *at*RA formation by recombinant enzymes and human liver S9 fractions. Retinaldehyde concentrations used in incubations were 0.2 (left column) and 1 μM (right column) while inhibitor concentrations (HDZ and WIN) were 250 μM in left panels and 500 μM in right panels. In panels A and B, inhibition assays were performed using recombinant human ALDH1A (open triangles) and AOX (open circles). In panels C-F, inhibition assays were done using HLS9 fractions and panels C and D show incubation s in the absence of NAD^+ while E and F show incubations in the presence of NAD^+. Bars represent mean values of three individual experiments performed on separate days while each data point represent an individual experiment done in duplicates. Different bars and symbols represent pooled HLS9 (filled gray bars) and HLS9 fractions from three individual donors (dashed, white and dotted bars). HDZ, hydralazine; WIN, WIN18,446.

Figure 5. Effects of CRBP1 on *at*RA formation by recombinant AOX, ALDH1A1 and human liver S9. Panel A shows *at*RA formation velocity when free retinaldehyde (-CRBP) or holo-CRBP1 (+CRABP) is used as a substrate. The bars represent the mean % inhibition from three individual experiments conducted on separate days and error bars represent S.D.. Panel B shows the predicted fraction of retinaldehyde metabolized by AOX and ALDH1A1 in the presence and absence of CRBP1. The substrate concentration (retinaldehyde or CRBP1-bound retinaldehyde) was 0.2 μM in all experiments.

DMD Fast Forward. Published on December 18, 2020 as DOI: 10.1124/dmd.120.000296
This article has not been copyedited and formatted. The final version may differ from this version.

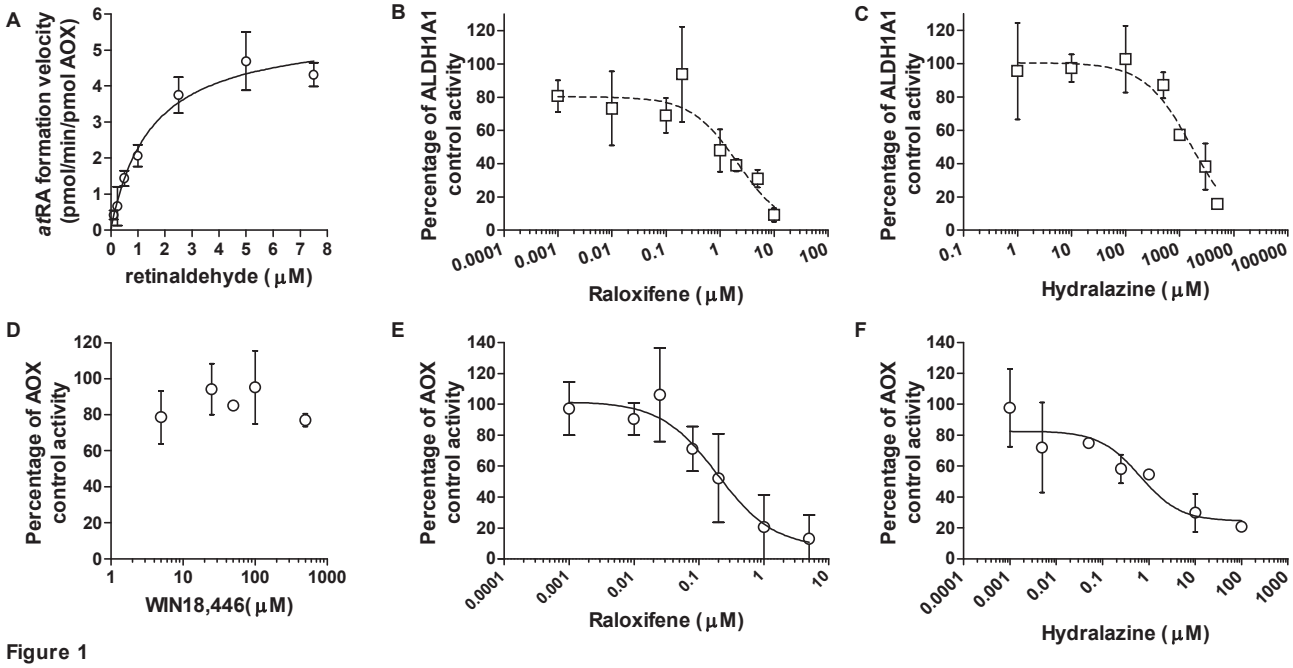

Figure 1

DMD Fast Forward. Published on December 18, 2020 as DOI: 10.1124/dmd.120.000296
This article has not been copyedited and formatted. The final version may differ from this version.

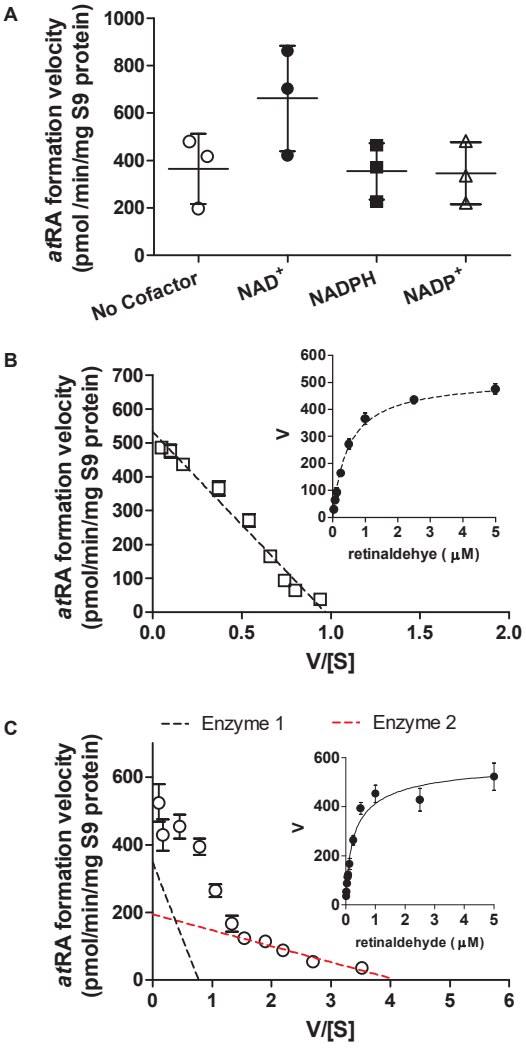

Figure 2

DMD Fast Forward. Published on December 18, 2020 as DOI: 10.1124/dmd.120.000296
This article has not been copyedited and formatted. The final version may differ from this version.

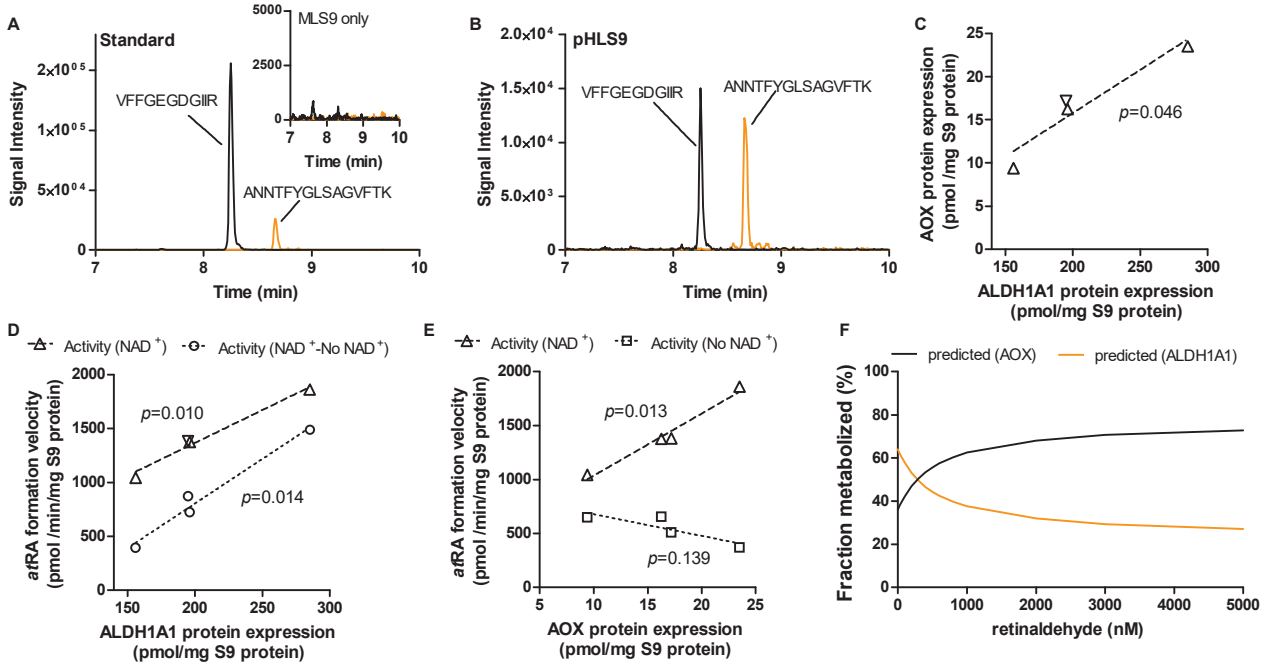

Figure 3

DMD Fast Forward. Published on December 18, 2020 as DOI: 10.1124/dmd.120.000296
This article has not been copyedited and formatted. The final version may differ from this version.

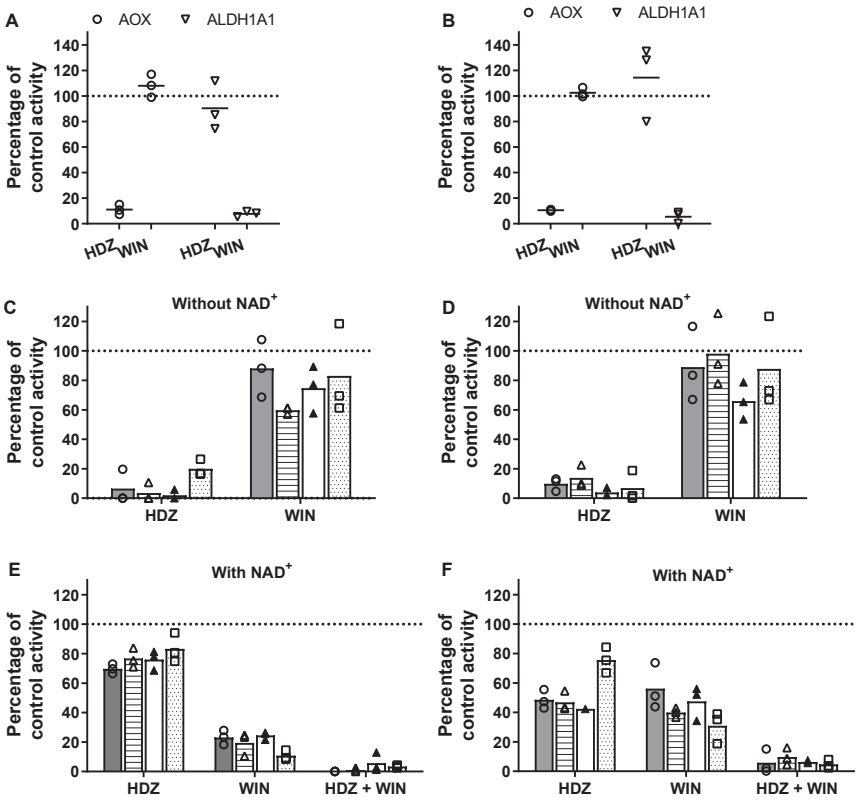

Figure 4

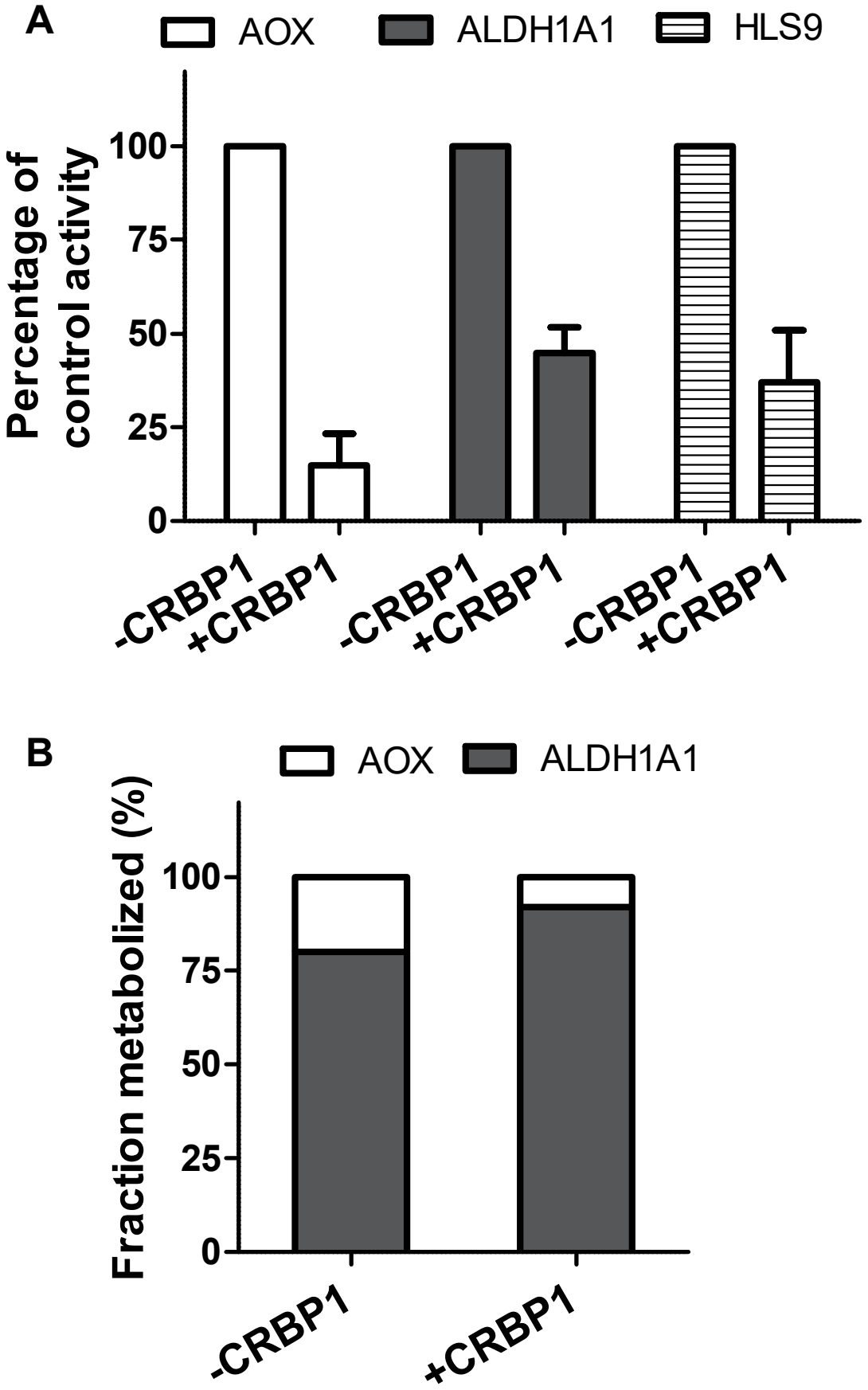
A
AOX
ALDH1A1
HLS9
Percentage of control activity
100
75
50
25
0
-CRBP1
+CRBP1
-CRBP1
+CRBP1
-CRBP1
+CRBP1
B
AOX
ALDH1A1
Fraction metabolized (%)
100
75
50
25
0
-CRBP1
+CRBP1

Figure 5